Electronic Supplementary Information

Theoretical study on Oxygen-modified phosphorene autogenous Z-scheme heterojunction for hydrogen evolution

Tianqi Zhang[+,a], Long Zhou[+,a], Guobo Chen[a], Shuwei Xia[*,a] and Meng Qiu[*,a]

[a] Key Laboratory of Marine Chemistry Theory and Technology (Ocean University of China), Ministry of Education, Qingdao 266100, China

I. Oxidation of black phosphorus

The optimized lattice parameters of monolayer black phosphorus are a=4.56 Å, b=3.32 Å, consistent with previous theoretical calculations (4.58 Å / 3.32 Å[1]), which proves the reliability of our calculation. Lattice parameters of the system increase with the increasing of O concentration; and the maximum lattice mismatch ratio between BP and PO_x lies in PO_1 (5.3%), which is admiring for their stacking as heterojunctions. In Fig. S1, PO_x skeletons still maintain folded structure after the adsorption of O, and O atoms extend to both sides; P atom closest to O atom was pulled up, leading to the increased distortion and deformation of BP framework. With the increase of O concentration, the deformation of BP becomes larger, and the largest deformation exists in PO_1. We predict that the structure should also be the most obvious in regulating the properties of black phosphorus, which is verified in Fig. S3. The details of bond lengths and bond angles are shown in Table S2.

The relative stabilities of all these structures are compared by binding energy, as:

$$Eb = \frac{1}{N_P + N_O}\left[E_{P+O} - (N_P E_P + N_o E_O)\right] \quad (1)$$

where N_O and N_P denote the number of O adatoms and phosphorus atoms in unit cell, respectively. In Eq. (1), E_{P+O}, E_P, and E_O are the energies of adatom adsorbed phosphorene monolayer, a single phosphorus and oxygen atom, respectively. Our calculated E_b of black phosphorus monolayer is -3.48 eV as shown in Table S1, which is consistent with previously reported value (-3.61 eV) [2-4], indicating the reliability of our calculation. In Table S1, all calculated binding energies are negative, indicating that the oxidized structures are thermodynamically stable. We found that the binding energy of PO_x decreased with the increase of O concentration, and the representative structure became more stable, which is consistent with the conclusions of Suhas Nahas et. al.[5] They also verified the thermal stability of these structures through molecular dynamics (MD) simulation, proving that these model could exist stably at ambient conditions. According to previous calculations[5], the configuration $PO_{0.5-3}$ owns the lowest energy and the most stable structure at the concentration of 0.5, this is consistent with E_b results; thus, we choose $PO_{0.5-3}$ to represent x=0.5 in this research.

In Fig. S3(c) (ESI†), the band gap of the system increases first and then decreases, reaches the maximum at the concentration of 0.5, which is consistent with Suhas' work; with the increase of O concentration, the band edge positions of valence band and conduction band gradually increase; the fermi energy level of the system decreases; the work function as a whole increase.
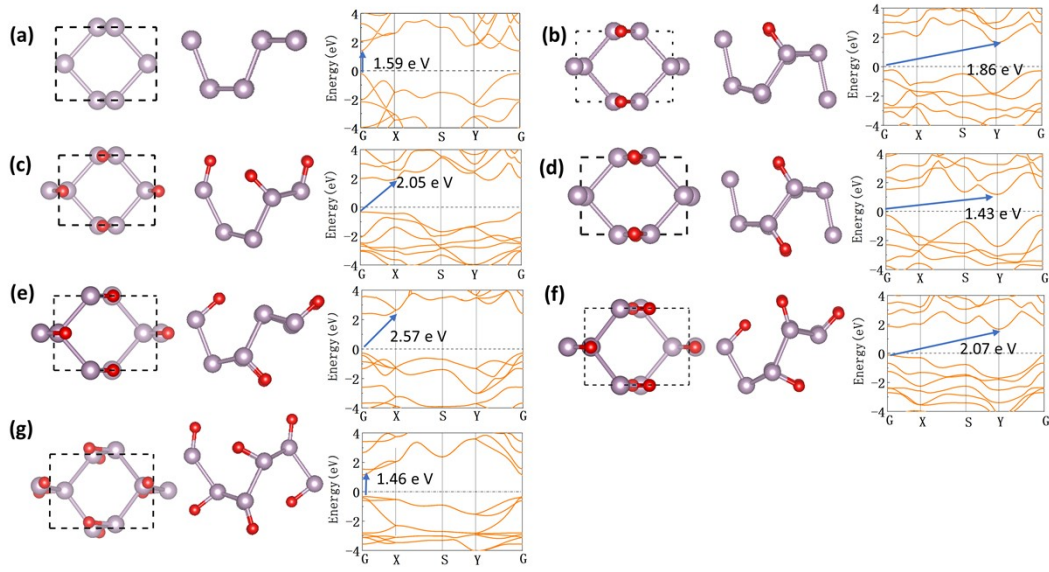
Fig. S1 Model construction and band structure of pristine and O-modified BP. Top view (left), side view (middle) and band structures calculated by HSE06 theoretical level (right; GGA results in Fig. S4) of (a) BP, (b) $PO_{0.25}$, (c) $PO_{0.5-1}$, (d) $PO_{0.5-2}$, (e) $PO_{0.5-3}$, (f) $PO_{0.75}$, (g) PO_1. The purple, and red spheres represent P and O atoms, respectively.
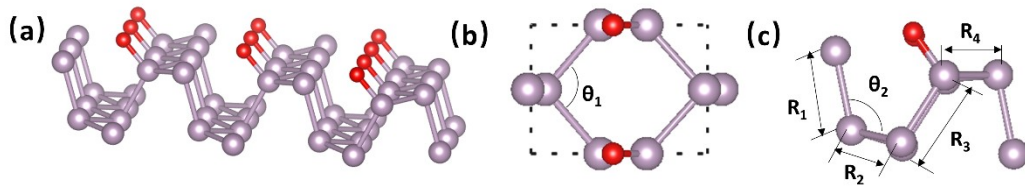

Fig .S2 The structure diagram of PO_x（a）The crystal structure of layered BP, (b) the top view of layered PO_x, (c) the side view of layered PO_x
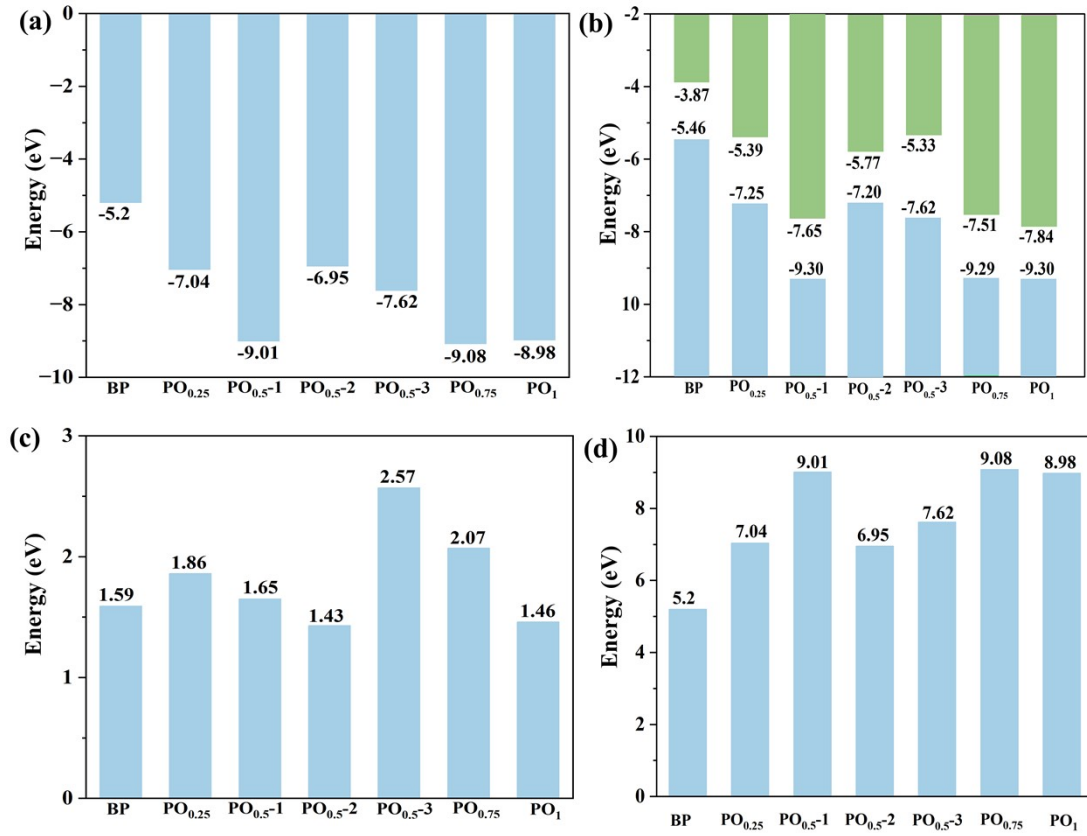
Fig. S3 Electronic structure of PO_x calculated by HSE06. (a) Fermi energy (b) band edge position (green represents the conduction band, blue represents the valence band) (c) band gap (d) work function

Table S1 The lattice parameters (a/b) and binding energy (E_b) of oxidized black phosphorus at different concentrations and sites (PO_x)

Configurations	a (Å）	b (Å)	E_b (eV)
BP	4.56	3.32[6]	-3.48
$PO_{0.25}$	4.64	3.35	-3.86
$PO_{0.5-1}$	4.82	3.46	-3.51
$PO_{0.5-2}$	4.75	3.42	-3.55
$PO_{0.5-3}$	4.70	3.39	-3.58
$PO_{0.75}$	4.79	3.51	-4.21
PO_1	5.05	3.62	-4.30

Table. S2 PO_x bond length and bond angle parameters

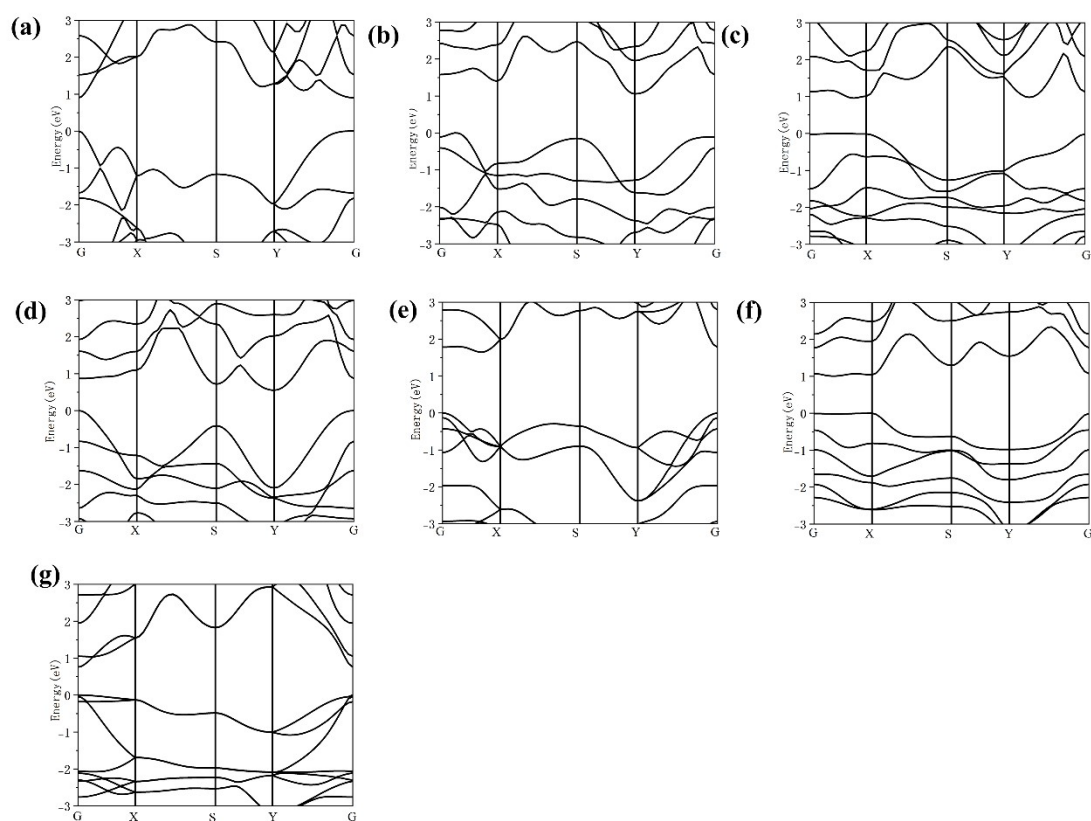| Configurations	R_1（Å）	R_2（Å）	R_3（Å）	R_4（Å）	θ_1	θ_2
Black phosphorus	2.25/2.24	2.23/2.28	2.25/2.24	2.23/2.28	96.46/96.00	103.63/103.51[1]
$PO_{0.25}$	2.28	2.24	2.25	2.25	96.16	107.32
$PO_{0.5-1}$	2.3	2.26	2.25	2.26	98.58	114.01
$PO_{0.5-2}$	2.26	2.27	2.24	2.27	97.47	98.76
$PO_{0.5-3}$	2.26	2.27	2.26	2.27	96.93	95.58
$PO_{0.75}$	2.24	2.23	2.33	2.23	99.12	90.67
PO_1	2.30	2.35	2.30	2.35	101.03	120.96

Fig. S4 GGA band structures of monolayer (a) BP, (b) $PO_{0.25}$, (c) $PO_{0.5-1}$, (d) $PO_{0.5-2}$, (e) $PO_{0.5-3}$, (f) $PO_{0.75}$, (g) PO_1
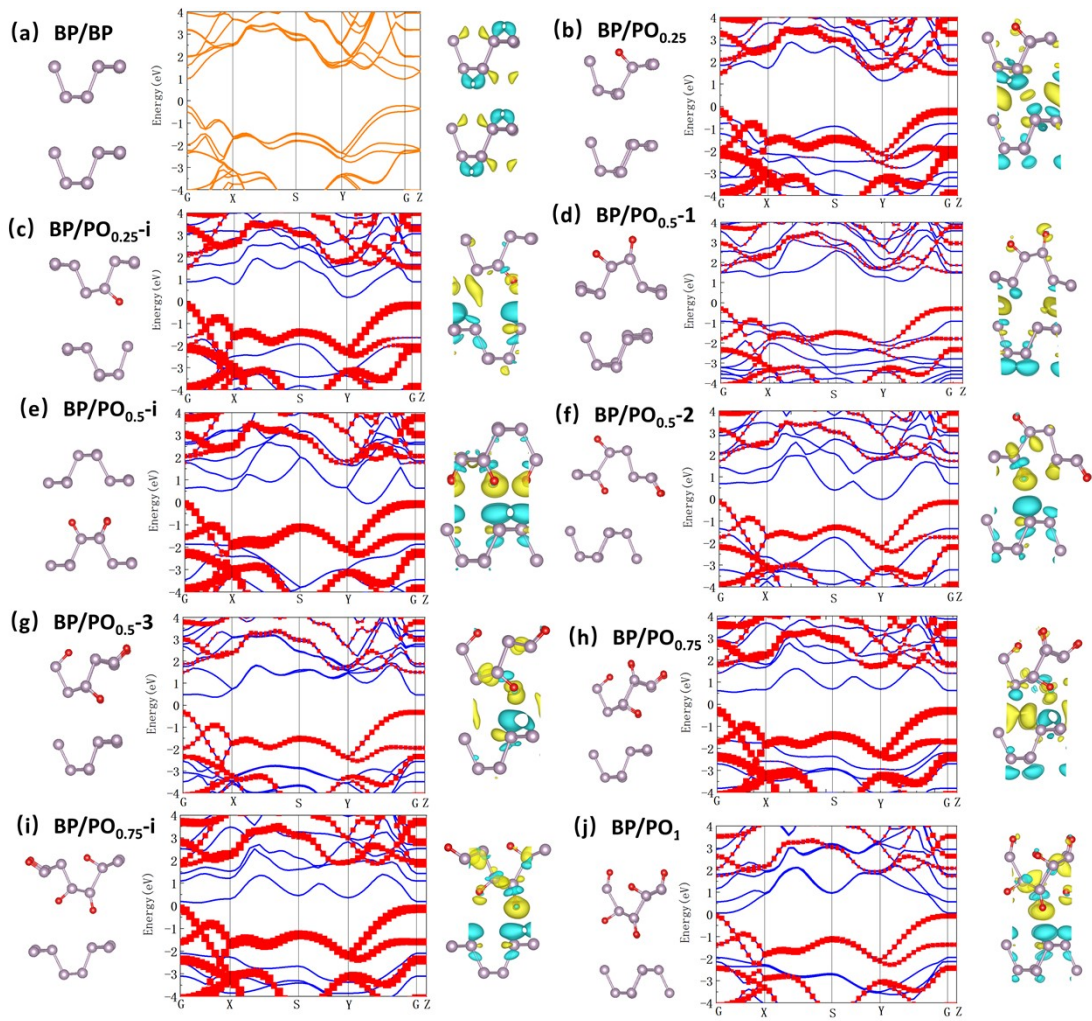
II. BP based Z-scheme heterojunction

Fig. S5 Model, band structure and Charge difference density of Heterostructures. Side view, energy band structure by HSE06 (BP and POx represented by red boxes and blue lines, respectively; GGA results in Fig. S9) and charge differential density diagram (yellow indicates electron accumulation and blue indicates electron dissipation) of (a) bilayer BP (b) BP/PO0.25 (c) BP/PO0.25 -i (d) BP/PO0.5 (e) BP/PO0.5-i (f) BP/PO0.5-2 (g) BP/PO0.5-3 (h) BP/PO0.75 (i) BP/PO0.75-i and (j) BP/PO1

Geometrical structure of bilayer black phosphorus were first optimized as a benchmark: its lattice parameters (a = 4.42 and b =3.32 Å) were close to previous calculated values (a = 4.52 and b = 3.33 Å[1]) ; the 1.25 eV bandgap also agreed well with the experimental values (1.29 eV)[7], indicating the accuracy of our computation. The bond length, bond angle and layer distance of double-layer black phosphorus are consistent with those reported in previous literature, also indicating the reliability of our calculation. Therefore, we used the same theoretical level to investigate our constructed heterostructures: deformation of the P framework in PO_x was more obvious than that of BP (mostly obvious in BP/PO_1 structure), and the change of O interlayers was more obvious than that of beyond layers. We speculate that intralayer oxygen will more significantly affect characters of heterojunction.

We used formation energy to judge the stability of the system, which is defined as follows:

$$E_f = E_{Het} - E_{BP} - E_{POx} \quad (2)$$

E_{Het}, E_{BP} and E_{POx} represent the energy of heterojunction, BP and PO_x monolayer, respectively. The formation energy E_f, interlayer distance d_{il}, and lattice parameters (a, b) of optimized heterostructures are summarized in Table S3. The E_fs were all negative for these configurations, indicating they are thermodynamically stable. We believe that it is possible to construct the heterojunction in an inert gas atmosphere.[8]
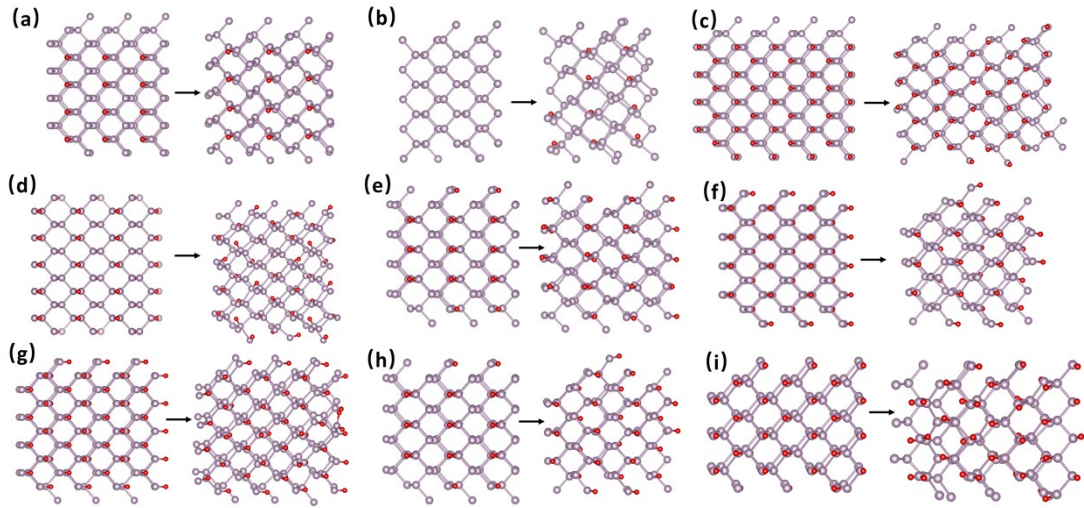
Fig. S6 The snapshots of the structures at 20 ps during AIMD simulations at 300K of (a) BP/PO$_{0.25}$ (b) BP/PO$_{0.25}$-i (c) BP/PO$_{0.5}$ (d) BP/PO$_{0.5}$-i (e) BP/PO$_{0.5}$-2 (f) BP/PO$_{0.5}$-3 (g) BP/PO$_{0.75}$ (h) BP/PO$_{0.75}$-i and (i) BP/PO$_1$

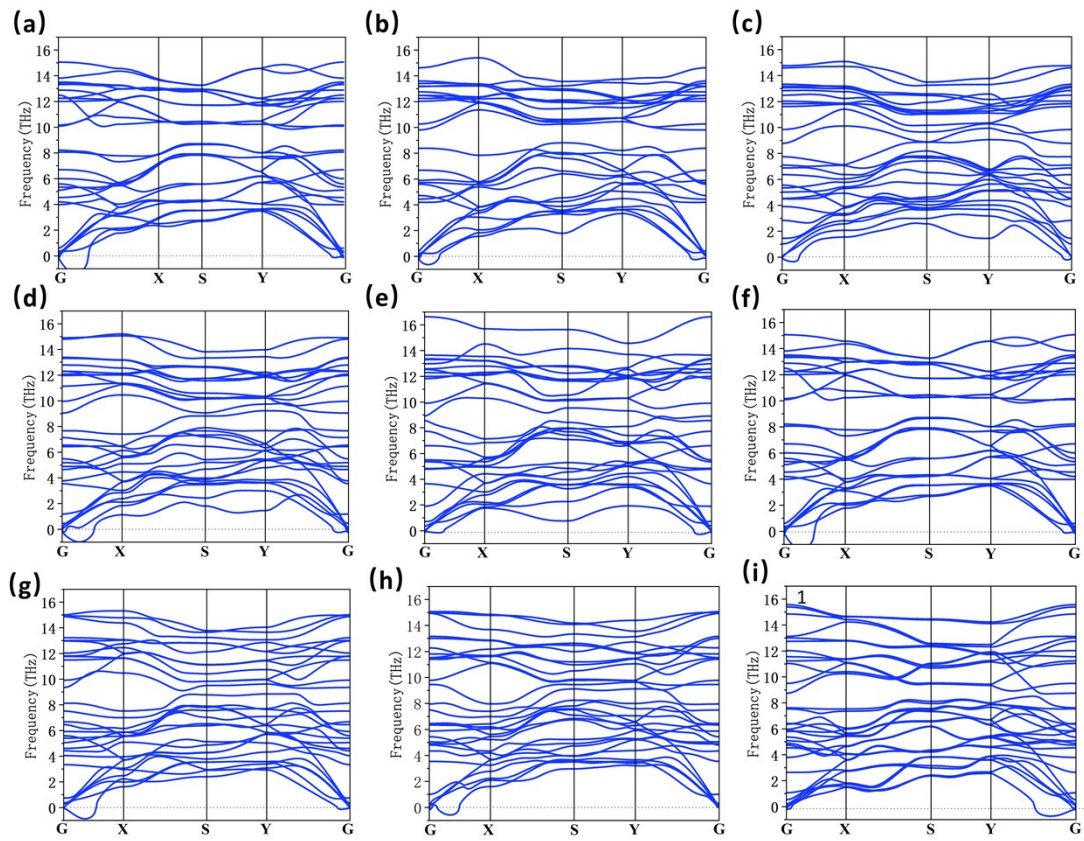

Fig. S7 The phonon dispersion along the high symmetrical directions of the Brillouin zone of (a) BP/PO$_{0.25}$ (b) BP/PO$_{0.25}$-i (c) BP/PO$_{0.5}$ (d) BP/PO$_{0.5}$-i (e) BP/PO$_{0.5}$-2 (f) BP/PO$_{0.5}$-3 (g) BP/PO$_{0.75}$ (h) BP/PO$_{0.75}$-i and (i) BP/PO$_1$

Table. S3 Lattice parameters and formation energy of Autogenous Z-scheme heterojunction

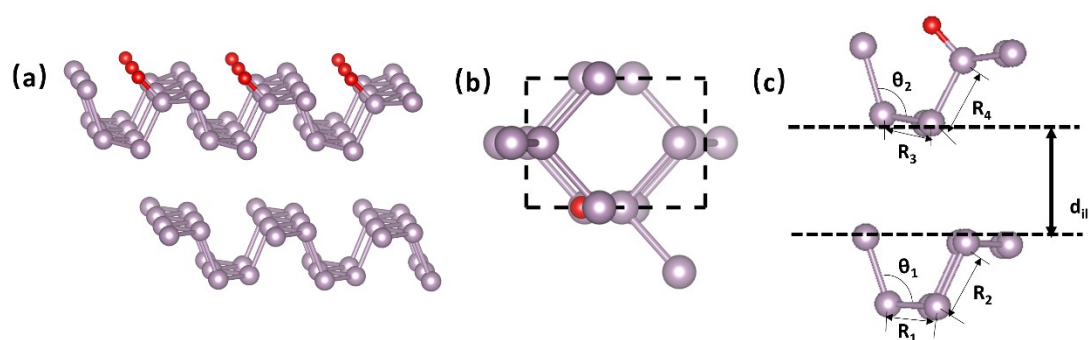| Configurations	a/b (Å）	d_{il} (Å)	E_f (eV)
bilayer BP	4.42/3.32	3.90	-1.12
BP/PO$_{0.25}$	4.62/3.33	3.76	-1.30
BP/PO$_{0.25}$-i	4.62/3.33	3.46	-1.03
BP/PO$_{0.5-1}$	4.65/3.38	3.49	-1.15
BP/PO$_{0.5}$-i	4.90/3.36	3.26	-1.71
BP/PO$_{0.5-2}$	4.73/3.35	3.47	-1.10
BP/PO$_{0.5-3}$	4.64/3.36	3.42	-1.26
BP/PO$_{0.75}$	4.73/3.41	3.34	-1.25
BP/PO$_{0.75}$-i	4.71/3.42	3.09	-0.91
BP/PO$_1$	4.83/3.46	3.12	-1.38

Fig. S8 The structure diagram of BP/PO$_x$（a) The crystal structure of layered BP, (b) the top view of layered PO$_x$, (c) the side view of layered PO$_x$
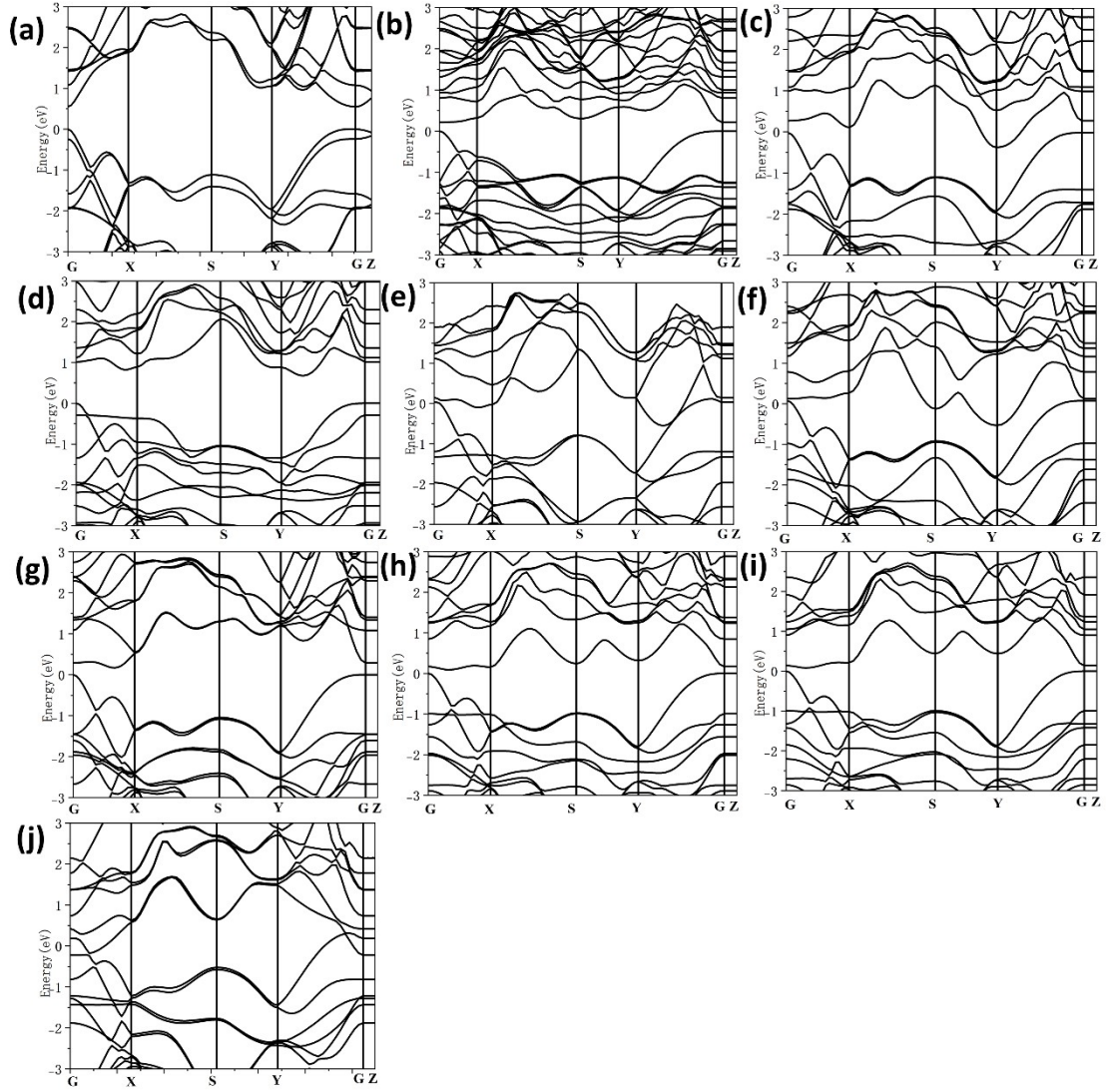
Fig. S9 GGA band structure of heterojunction (a) bilayer black phosphorus (b) BP/PO$_{0.25}$ (c) BP/PO$_{0.25}$ -i(d) BP/PO$_{0.5}$ (e) BP/PO$_{0.5}$-i (f) BP/PO$_{0.5}$-2 (g) BP/PO$_{0.5}$-3 (h) BP/PO$_{0.75}$ (i) BP/PO$_{0.75}$-i and (j) BP/PO$_1$

The calculation formula of the differential charge density is:

$$\Delta\rho = \rho_{BP/POx} - \rho_{BP} - \rho_{POx} \quad (3)$$

The $\rho_{BP/POx}$, ρ_{BP} and ρ_{POx} represent the differential charge density of heterojunction, BP and PO$_x$, respectively.

Table. S4 Z-scheme heterojunction bond length and bond angle parameters

Configurations	R_1 (Å)	R_2 (Å)	R_3 (Å)	R_4 (Å)	θ_1	θ_2
Bilayer BP	2.22/2.24	2.26/2.28	2.22/2.24	2.26/2.28	102.53/102.96	102.53/102.96[1]
BP/PO$_{0.25}$	2.23	2.26	2.23	2.25	104.42	107.58
BP/PO$_{0.25}$-i	2.23	2.25	2.24	2.24	103.92	107.39
BP/PO$_{0.5-1}$	2.24	2.26	2.25	2.24	104.29	114.10
BP/PO$_{0.5}$-i	2.23	2.26	2.25	2.25	105.19	101.40
BP/PO$_{0.5-2}$	2.23	2.28	2.26	2.23	106.49	106.99
BP/PO$_{0.5-3}$	2.24	2.25	2.25	2.26	104.65	95.28
BP/PO$_{0.75}$	2.25	2.26	2.27	2.33	104.93	89.74
BP/PO$_{0.75}$-i	2.25	2.26	2.26	2.31	104.47	90.12
BP/PO$_1$	2.26	2.27	2.27	2.26	106.13	121.66

Table S5 Electronic properties, effective mass, charge transfer and formation energy of the constructed Z-scheme heterojunction

| Configurations	VBM (eV)	CBM (eV)	Band gap (eV)	Fermi energy (eV)	Work function (eV)	Electronic effective mass (m_0)	Bader	Formation energy (eV)
bilayer BP	-5.20	-3.95	1.25	-0.18	5.07	0.26/4.50	0	-1.15
PO$_{0.25}$/BP	-6.78	-5.40	1.38	-0.96	6.55	0.52/3.70	0.01	-1.30
PO$_{0.25}$-i/BP	-5.47	-5.10	0.37	-0.03	5.29	0.58/1.52	0.03	-1.03
PO$_{0.5-1}$/BP	-8.29	-6.92	1.37	0.26	8.00	0.87/1.633	0.02	-1.15
PO$_{0.5}$-i/BP	-6.39	-6.36	0.03	-0.09	6.31	0.46/1.14	0.15	-1.71
PO$_{0.5-2}$/BP	-5.74	-5.61	0.13	-0.49	5.59	1.58/2.27	0.06	-1.10
PO$_{0.5-3}$/BP	-5.68	-4.99	0.69	-0.06	5.36	0.91/0.65	0.04	-1.26
PO$_{0.75}$/BP	-7.82	-6.97	0.85	-0.84	7.52	0.67/0.53	0.02	-1.25
PO$_{0.75}$-i/BP	-6.12	-5.90	0.27	-0.04	6.04	1.63/0.54	0.11	-0.91
PO$_1$/BP	-7.15	-7.01	0.22	-1.11	7.08	0.18/1.06	0.12	-1.38
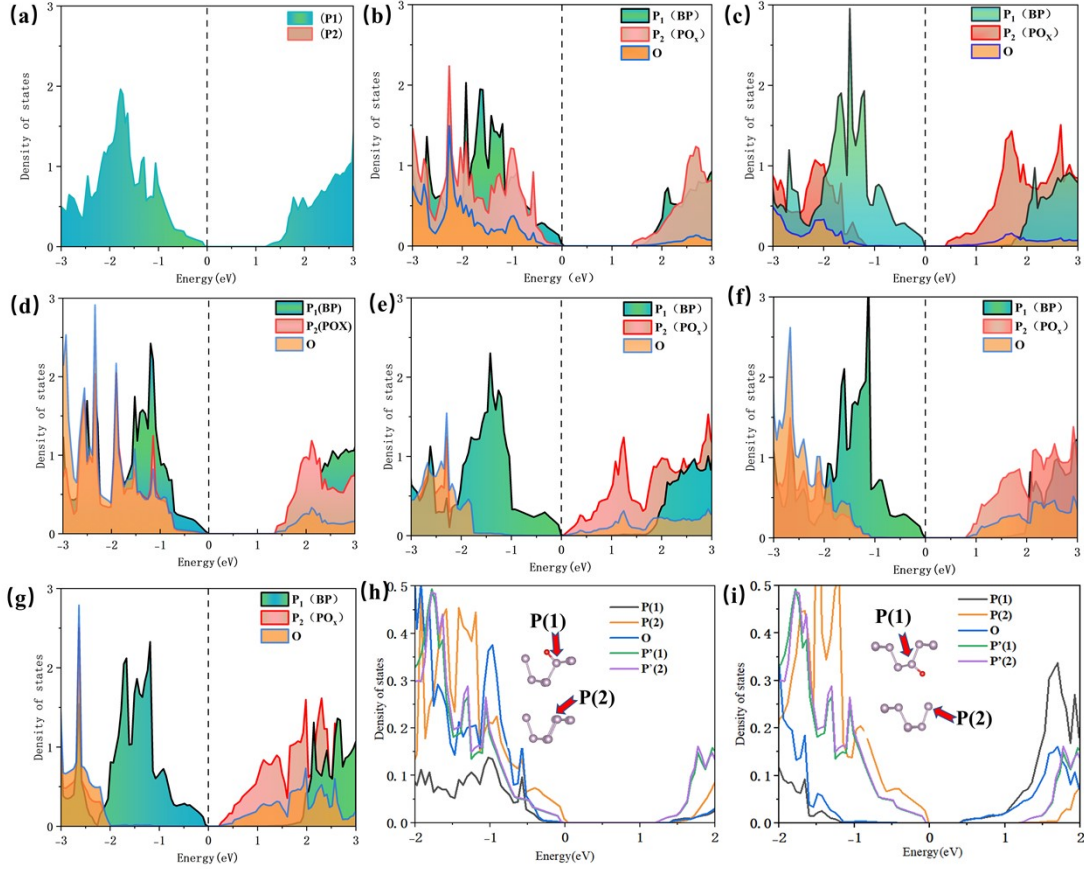
Fig. S10 The PDOS for the bilayer BP and heterojunctions calculated by HSE06. (a) bilayer BP (b) BP/PO$_{0.25}$ (c) BP/PO$_{0.25}$ -i (d) BP/PO$_{0.5}$ (e) BP/PO$_{0.5}$-i (f) BP/PO$_{0.75}$ (g) BP/PO$_{0.75}$-i (h) BP/PO$_{0.25}$ (i) BP/PO$_{0.25}$ -i; P' (1) and P' (2) are the corresponding P atoms, comparing to PO$_{0.25}$, in bilayer BP

Light absorption calculation details

The nonlinear optical intersubband absorption coefficient of a material is associated with its photocatalysis, photovoltaics, and optoelectronics. The coefficient can be calculated from the following equation[9]:

$$\alpha(\omega) = \sqrt{2}\,\omega\sqrt{\sqrt{\varepsilon_1^2(\omega) + \varepsilon_2^2(\omega)} - \varepsilon_1(\omega)}\,(4)$$

the dielectric function $\varepsilon_2(\omega)$ was calculated as follows[10]:

$$\varepsilon_2(\omega) = \frac{4\pi}{m^2\omega^2}2\sum_{c,v}\int_{BZ}\frac{2}{(2\pi)^3}|M_{c,v}(k)|^2\delta\left(\varepsilon_{ck} - \varepsilon_{vk} - h\omega\right)d^3k\,(5)$$

where $|M_{c,v}(k)|^2$ is the momentum matrix element, and c and v represent the conduction and valence states, respectively. The real part $\varepsilon_1(\omega)$ is derived from the imaginary part by Kramers–Kronig transformation.
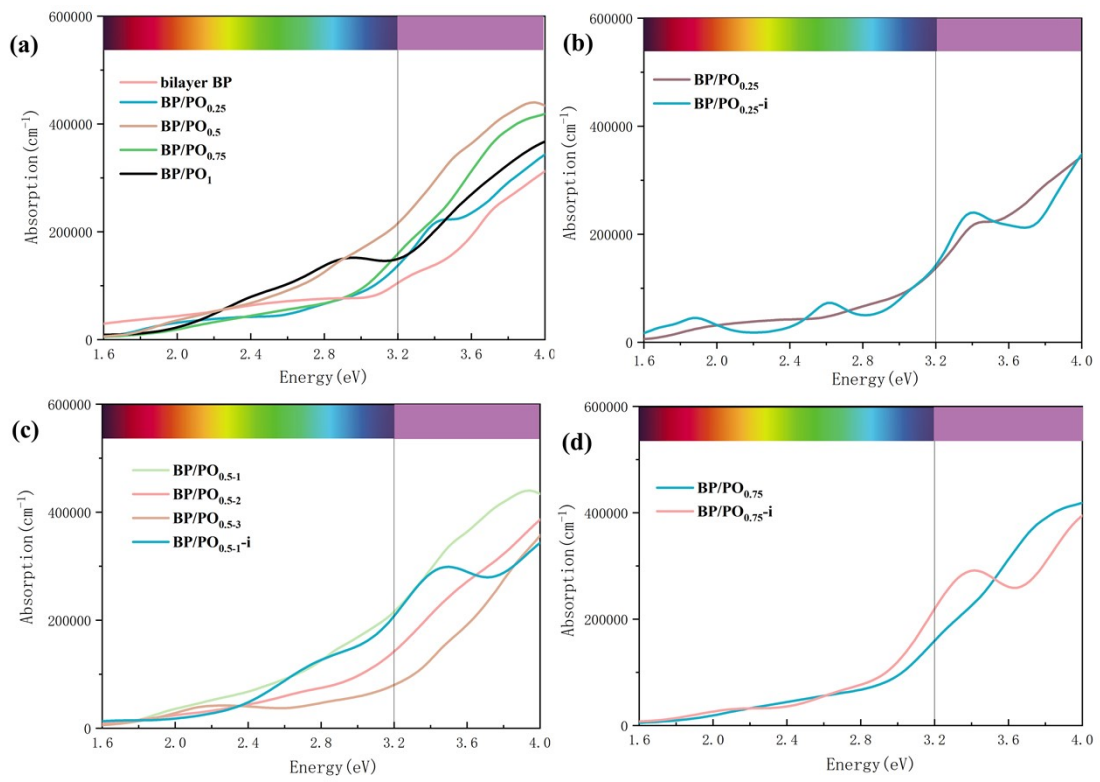
Fig. S11 Comparison diagram of light absorption at different concentrations, configurations and O adsorption sites
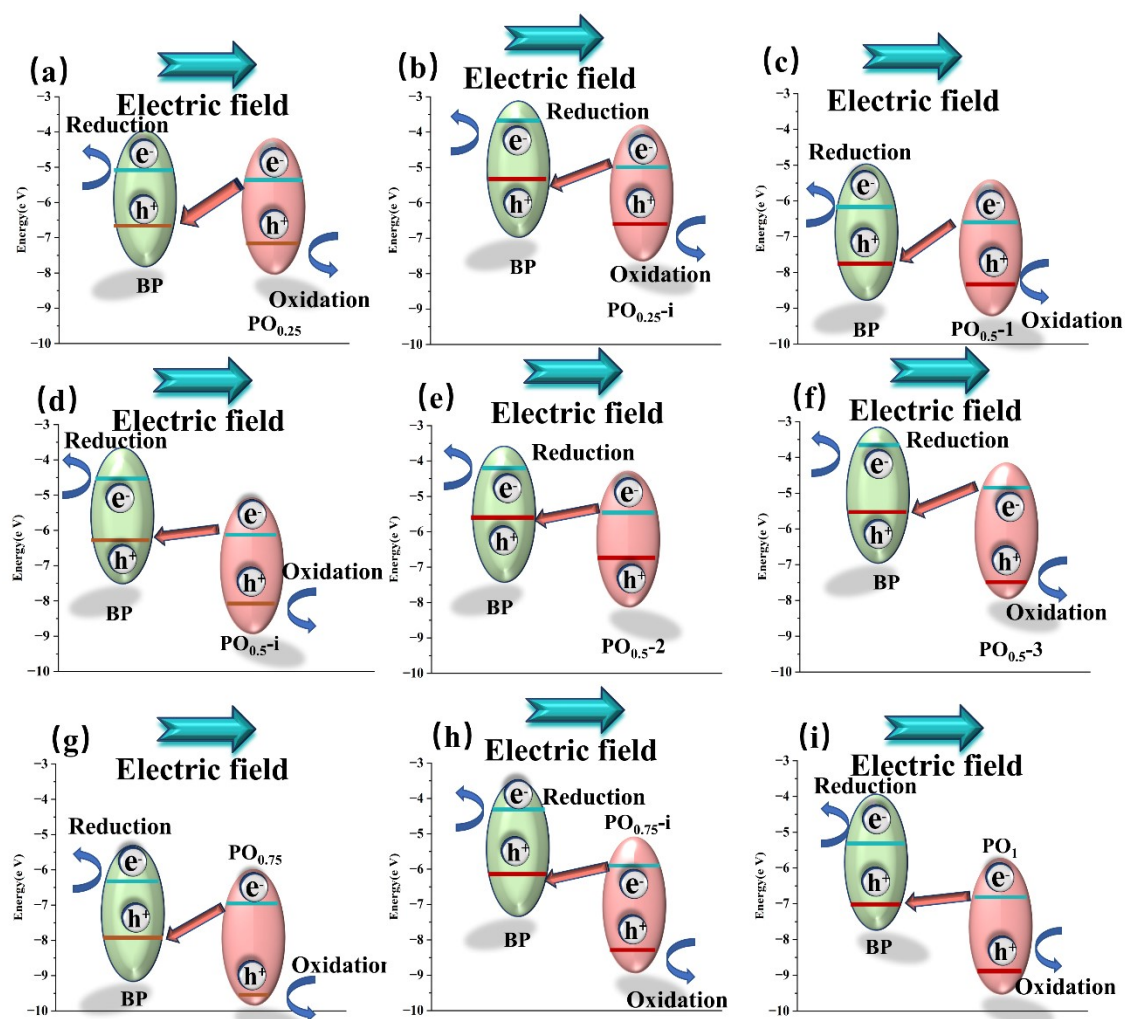
The heterojunction principle and redox potential

Fig. S12 The band alignments and built-in field of Z-schemes BP/PO_x heterostructure (a) $BP/PO_{0.25}$ (b) $BP/PO_{0.25}$-i (c) $BP/PO_{0.5}$ (d) $BP/PO_{0.5}$-i (e) $BP/PO_{0.5}$-2 (f) $BP/PO_{0.5}$-3 (g) $BP/PO_{0.75}$ (h) $BP/PO_{0.75}$-i (i) BP/PO_1

The energy levels (valence band maximum and conduction band minimum) of BP and PO_x are interlaced with each other when they constitute the 2D BP/PO_x heterostructure. Both of BP and PO_x can generate electrons and holes in their CB and VB under light irradiation, respectively; while photogenerated electrons in the CB of PO_x would move into the VB of BP to combine photo-generated holes in Fig. S12(ESI†). This recombination can promote the separation of photo-induced carriers of the system, resulting in more photogenerated electrons at the CBM of BP and more photogenerated holes at the VBM of PO_x. Consequently, net photogenerated carriers were located at BP and PO_x, respectively. Besides, the direct Z-scheme heterostructure can form a more negative potential of the CBM and more positive potential of the VBM, achieving a strong reduction and oxidation ability compared to traditional type II heterostructures. The redox potential in Z-scheme heterojunction is located at the top of the valence band of PO_x and the bottom of the conduction band of BP respectively. As shown in Fig. 3，we found that the oxidation potentials of the nine heterojunctions constructed were all higher than 1.23 V (standard hydrogen electrode, SHE), indicating that the nine heterojunctions can be used in OER reaction; in terms of reduction potential, the reduction potentials of the four structures ($BP/PO_{0.25}$-i, $BP/PO_{0.5}$-2, $BP/PO_{0.5}$-3 and $BP/PO_{0.75}$-i) are lower than 0 V, indicating

that the photocatalytic HER reaction can be carried out spontaneously. Hydrogen evolution reaction (HER), the simplest catalytic reaction, was used to further elucidate the performance of BP/PO$_x$ heterostructure.
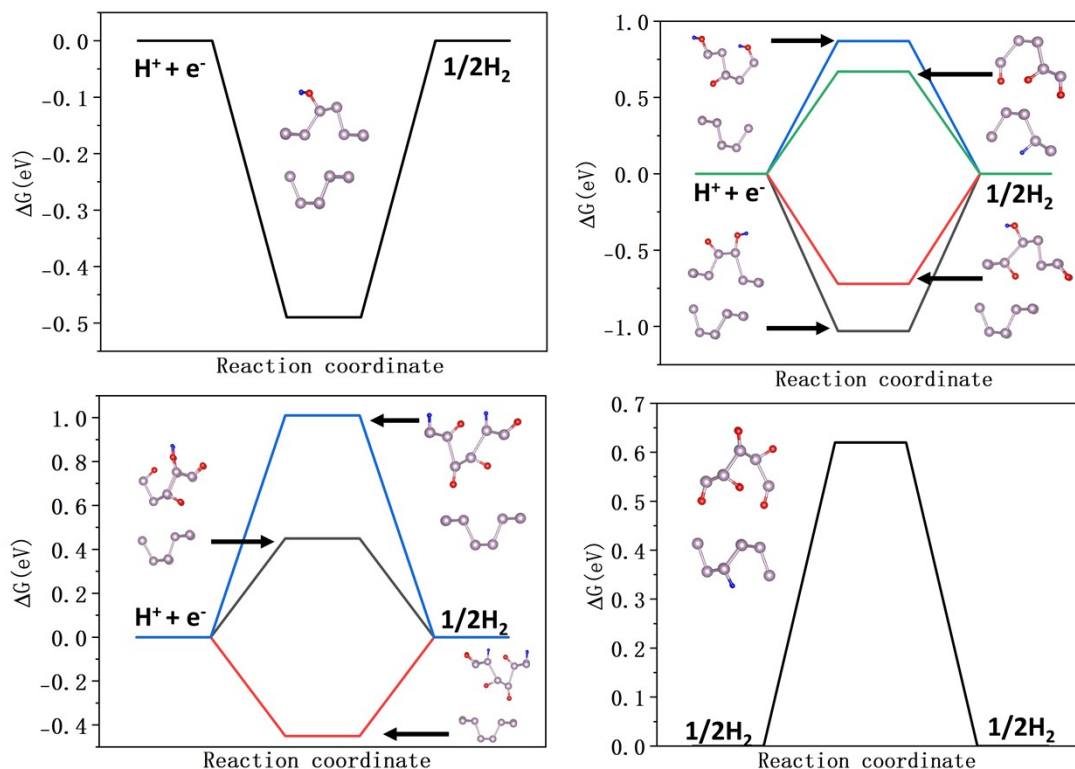

Fig. S13 The Gibbs free energies of the HER at different adsorption sites on the BP/PO$_x$. The hydrogen atoms absorbed on the heterostructures are represented with H* and labeled blue

Reference

1. J. Qiao, X. Kong, Z.-X. Hu, F. Yang and W. Ji, *Nature communications*, 2014, **5**, 1-7.
2. Y. Wang, F. Li, Y. Li and Z. Chen, *Nature communications*, 2016, **7**, 1-7.
3. H. Liu, A. T. Neal, Z. Zhu, Z. Luo, X. Xu, D. Tománek and P. D. Ye, *ACS nano*, 2014, **8**, 4033-4041.
4. L. Li, Y. Yu, G. J. Ye, Q. Ge, X. Ou, H. Wu, D. Feng, X. H. Chen and Y. Zhang, *Nature nanotechnology*, 2014, **9**, 372-377.
5. S. Nahas, B. Ghosh, S. Bhowmick and A. Agarwal, *Physical Review B*, 2016, **93**, 165413.
6. B. Li, C. Lai, G. Zeng, D. Huang, L. Qin, M. Zhang, M. Cheng, X. Liu, H. Yi, C. Zhou, F. Huang, S. Liu and Y. Fu, *Small*, 2019, **15**, e1804565.
7. B. Li, C. Lai, G. Zeng, D. Huang, L. Qin, M. Zhang, M. Cheng, X. Liu, H. Yi and C. Zhou, *Small*, 2019, **15**, 1804565.
8. L. Chen, G. Su, C. Wang, L. Dang and H. Wei, *Separation and Purification Technology*, 2022, **292**, 120986.
9. S. Saha, T. Sinha and A. Mookerjee, *Physical Review B*, 2000, **62**, 8828.
10. A. Read and R. Needs, *Physical Review B*, 1991, **44**, 13071.